RESEARCH ARTICLE

Correspondence to:
G. Alendal,
guttorm.alendal@uib.no

Simulating spatial and temporal varying CO_2 signals from sources at the seafloor to help designing risk-based monitoring programs

Alfatih Ali[1], Håvard G. Frøysa[1], Helge Avlesen[2], and Guttorm Alendal[1]

[1]Department of Mathematics, University of Bergen, Bergen, Norway, [2]Uni Research Computing, Bergen, Norway

Abstract Risk-based monitoring requires quantification of the probability of the design to detect the potentially adverse events. A component in designing the monitoring program will be to predict the varying signal caused by an event, here detection of a gas seep through the seafloor from an unknown location. The Bergen Ocean Model (BOM) is used to simulate dispersion of CO_2 leaking from different locations in the North Sea, focusing on temporal and spatial variability of the CO_2 concentration. It is shown that the statistical footprint depends on seep location and that this will have to be accounted for in designing a network of sensors with highest probability of detecting a seep. As a consequence, heterogeneous probabilistic predictions of CO_2 footprints should be available to subsea geological CO_2 storage projects in order to meet regulations.

1. Introduction

The legal regulations for geological storage, e.g., the EU directive 2009/31/EC, establishes a legal framework for geological storage of CO_2, eliminating as far as possible negative effects and environmental risks. Offshore these regulations are aligned with the amendments to the 1996 London Protocol and to the OSPAR Convention. An intrinsic part of the imposed requirements is an adequate monitoring program.

With proper selection and operational procedures, CO_2 geological storage projects will be designed not to leak. A number of different trapping mechanisms will keep the injected and buoyant CO_2 inside the intended formation [*Rutqvist*, 2012], with the injection well as the most probable leakage pathway. However, transport of the CO_2 within the formation might cause other pathways to the surface to become probable, or the CO_2 might create new pathways, possibly far away from the injection well [*Oldenburg and Lewicki*, 2006].

Even if the formation and the overburden are monitored, there will be uncertainties in the quantification of CO_2 contained within the formation. And, what is the detection limit of CO_2 migrating toward the surface possibly through unknown pathways to the surface? These questions can only be answered within a certain degree of certainty.

Due to this, there is a need and requirement for a surface monitoring program with three main objectives; (1) assure that a leak will most likely be detected, (2) continue to build an accurate baseline to capture trends and natural variability, and (3) to prevent unjustified accusations of adverse effects from the storage project. The 2011 incident at the Weyburn project is an example of the latter [*Boyd et al.*, 2013].

For offshore storage projects such a monitoring program will be costly and the marine environment is hostile for instrumentations. We therefore suggest that the monitoring program has three levels of modus operandi; (1) detection modus, (2) location modus, and (3) quantification modus. The three modes will have different needs with regard to instrumentation and data; for instance location mode will require current predictions in real time to be able to move upstream from any signal, as opposed to the statistical current conditions that is sufficient for the detection modus.

Two main building blocks are necessary in order to build a monitoring program that optimize the probability of detecting a leak [*Hvidevold et al.*, 2015]: (1) a map of probable leak locations, preferably quantifying the internal relative probability between the different sites. Only a thorough site characterization of the

underburden can accomplish this. (2) Probable footprints of a seep to the water column, which have to be achieved through modeling.

CO_2 entering the water column will rise either as liquid droplets deeper than $\sim$500 m, or gas bubbles shallower than $\sim$ 500 m [*Alendal and Drange*, 2001]. In the shallow regime, a seep will create individual bubbles, bubble trains, or bubble plumes if the flux rate is high enough. The dynamics of these regimes are different, with the plume dynamics being the most challenging to model due to the two-way dynamic coupling between bubble movement and dissolution and the resulting dense plume water [*Alendal and Drange*, 2001; *Sato and Sato*, 2002; *Chen et al.*, 2003; *Dewar et al.*, 2013, 2015].

Detection of bubbles can be made from sonars [*Brewer et al.*, 2006; *Noble et al.*, 2012]. It will be necessary to distinguish between natural occurring seeps and seeps originating from the storage site. Another indication of a leak might be environmental impact caused by elevated CO_2 concentration in the vicinity of the source [*Blackford et al.*, 2010], especially through changes in bottom fauna such as new occurrences of bacterial mats [*Wegener et al.*, 2008].

The purpose here is to simulate spatial and temporal signals of elevated CO_2 concentration away from the seep location and illustrate which impact this variability will have on the design of a monitoring program using chemical sensors. The footprints are mainly governed by the varying, both spatially and temporally, current conditions. The direction and amplitude of the current follows the tidal signal [*Davies and Furnes*, 1980], and atmospheric forcing and local topography might cause the expected anisotropic footprint of a CO_2 leak [*Alendal et al.*, 2005].

A statistical baseline of important environmental parameters, e.g., currents, natural gas seeps, and biogeochemical parameters, is required for designing a comprehensive monitoring program. Historical data are important in combination with new data collected during site characterization. Long-time series are important in order to capture natural variability, such as seasonal changes and long-term trends. In particular it will be important to capture the expected increase of CO_2 concentration caused by the acidification of marine waters [*Caldeira and Wickett*, 2003].

In a recent EU FP7 project, ECO2, a number of leak scenarios in the central North Sea were defined [*Blackford et al.*, 2012]. Two of these scenarios, the chimney reactivation and seeps through a fault or fracture, were studied further with focus on processes and transport of the CO_2 once it reached the water column [*Alendal et al.*, 2014]. The estimated maximum CO_2 flux rates through the seafloor were, respectively, 150 ton/d and 15 ton/d for these two scenarios.

Among the models used was the high-resolution Heriot-Watt University (HWU) two-fluid bubble plume model [*Dewar et al.*, 2013, 2015]. The bubble plumes were simulated with different, but constant, characteristics background currents speeds characteristic for the central North Sea. These simulations showed that a constant vertical profile of the dissolved CO_2 is a reasonable assumption, i.e., independent of background current speed [*Alendal et al.*, 2014].

On a larger scale, i.e., when the CO_2 concentration becomes diluted and hence a dynamically passive tracer, transport of the seeped CO_2 was simulated by an 800 m resolution North Sea set up of the Bergen Ocean Model (BOM). Based on the vertical profiles obtained by the high-resolution bubble plume model, the seep was implemented as source terms distributing the CO_2 in a single vertical array.

Hvidevold et al. [2015] used one of the scenarios and a simplified map of the North Sea, identifying wells and formations, to optimize locations of chemical sensors. It was shown that placing the sensors successively at the location of highest probability is not necessarily the best option. One sensor might detect seeps at several potential leak locations. The need for a proper baseline to reduce the threshold for a statistically significant signal was demonstrated by comparing the threshold obtained after applying the stoichiometric approach described in *Botnen et al.* [2015] with natural variability. The design framework presented in *Hvidevold et al.* [2015] allows to quantify the uncertainty when claiming no leakage occurs.

In a follow-up study *Hvidevold et al.* [2015] used time series from the same GCM predictions accounting for temporal variability. There is no reason to wait until the temporal average concentration is statistically significant to sound an alarm, but rather when events of higher concentration becomes frequent enough and with high enough amplitude. This changed approach increased the area covered by an individual sensor
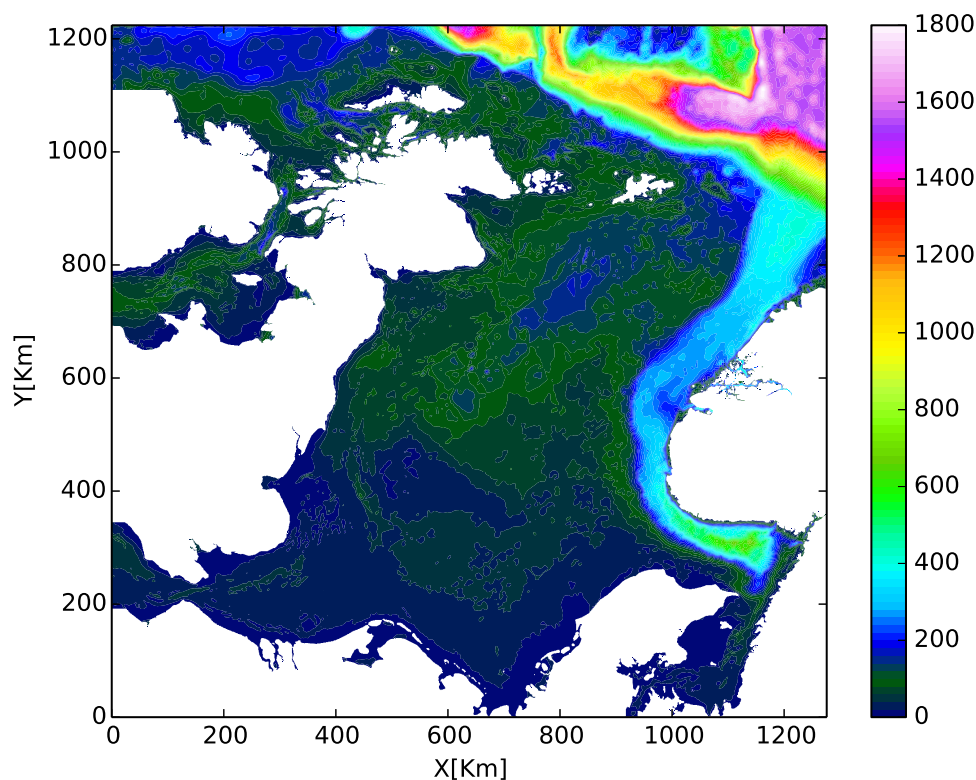
Figure 1. The model area covers the North Sea and the color represents the bathymetry in meter. The model area is located between latitudes 50°N and 64°N and longitudes 12°W and 10°E.

remarkably. These time series also opened for calculating the probability of the concentration to be above a threshold value at any given time and time from leak start to detection [*Greenwood et al.*, 2015]. As a consequence cruise-based monitoring, i.e., a series of individual measurements taken at different locations was also demonstrated. Including optimal routing of such cruises.

The natural next step is to study how the footprint characteristics changes with seep location, which is the purpose of the present study. The 800 m grid resolution North Sea setup of the three-dimensional terrain-following Bergen Ocean Model (BOM) is used to transport and disperse CO_2 from nine different locations, predicting spatial concentration time series for each of the seeps individually. How footprint predictions dependency on leak location influence monitor design is demonstrated through a simplified scenario.

2. Setup and Forcing of Bergen Ocean Model

The Bergen Ocean Model (BOM) is a three-dimensional terrain-following nonhydrostatic ocean model with capabilities of resolving mesoscale to large-scale processes. The model code is implemented in modern Fortran, with freely available source from http://www.mi.uib.no/BOM/. For further information on BOM, see the user's guide [*Berntsen*, 2004]. The governing equations are the Reynolds momentum equations with the Boussinesq approximation. In this study, the hydrostatic version of the model is used.

A number of studies have been conducted to evaluate BOM. *Berntsen and Svendsen* [1999] compared simulations with the SKAGEX North Sea data set and in *Berntsen et al*. [2006, 2008, 2009] properties of internal waves at sills in Loch Etive were studied, including comparisons with measurements. On laboratory scale, *Berntsen et al*. [2006] and *Thiem et al*. [2011] compared simulations to experiments for the lock release problem and for solitary internal waves. *Rygg et al*. [2011] compared BOM with theory and the MITgcm for flow over backward facing step.

The model area in this study covers the North Sea as shown in Figure 1. The horizontal grid resolution is 800 m and 41 σ-coordinate layers are used in the vertical, with a vertical resolution of less than 1 m in the
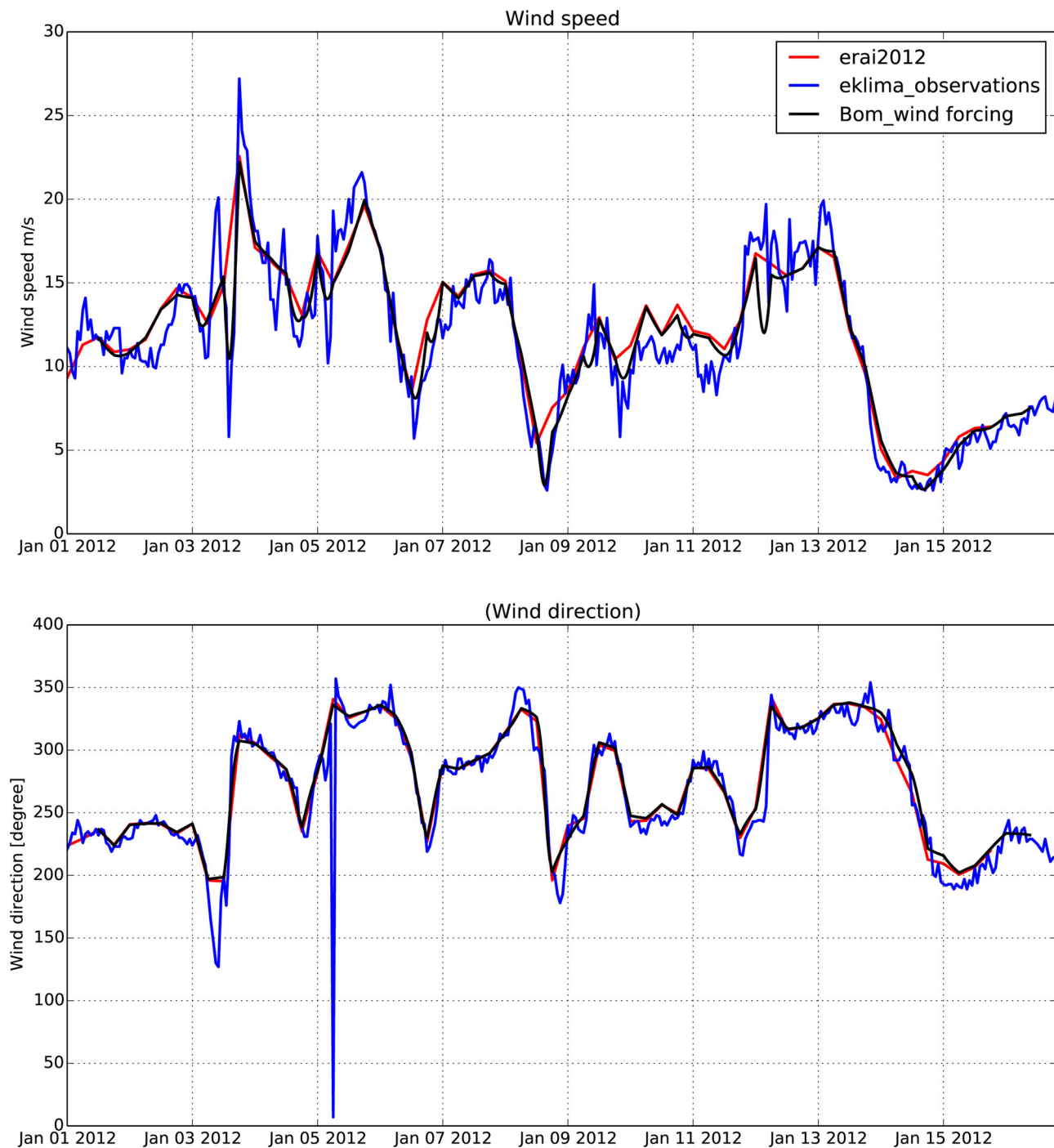
Figure 2. (top) Wind speed, and (bottom) wind direction time series at Sleipner A in the period 1–15 January 2012. Blue line is the observation from eklima **www.met.no** and red line is the data from erai reanalysis, while black line is interpolated wind forcing in BOM from erai-2012.

shallow areas, and up to tens of meters in the middle of the water column in deeper areas. This discretization gives 1595 and 1530 grid points in *x* and *y* direction, respectively. The model forcing data consist of wind, atmospheric pressure, harmonic tides, rivers, and initial fields for salinity and temperature.

Water elevation and velocities are spun up from zero. Initial values and lateral boundary conditions of temperature and salinity are taken from the UK Metoffice FOAM 7 km model published by MyOCEAN service at *http://www.myocean.eu.org/*, and interpolated into the model grid. So the model is close to being a one way nested submodel of FOAM.
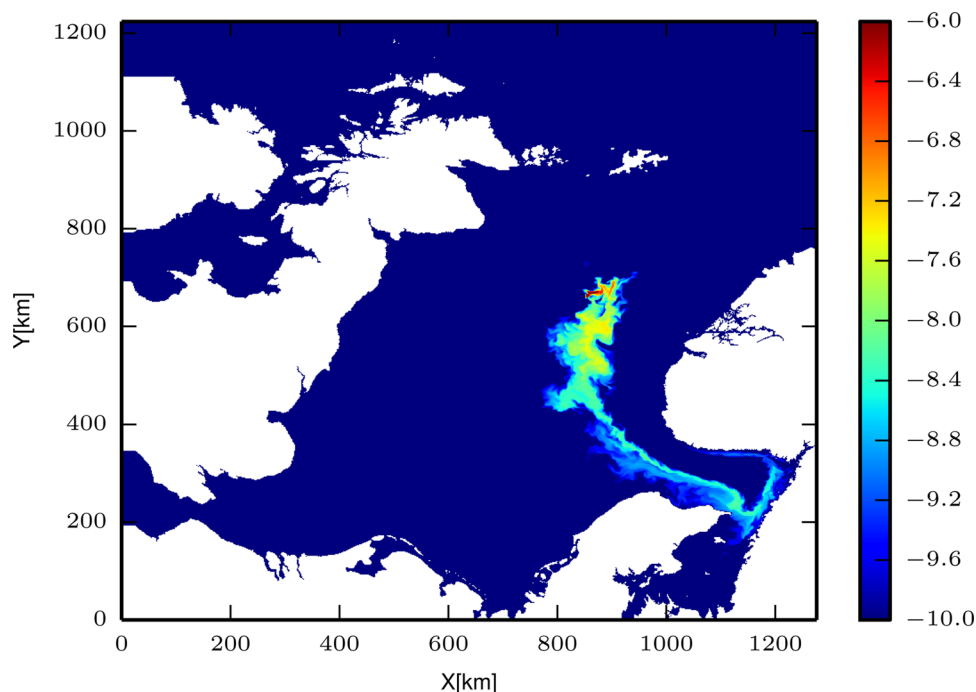
Figure 3. Release of a passive tracer at Sleipner A. The color is in a logarithmic scale. We observe that the tracer follows the observed current pattern in the North Sea [*Rodhe*, 1998; *Otto* et al., 1990; *Winther and Johannessen*, 2006].

The boundary conditions are implemented using the Flow Relaxation Scheme (FRS) described in *Martinsen and Engedahl* [1987], using 31 grid cells wide flow relaxation zones at open boundaries.

The atmospheric forcing data are collected and interpolated from The European Centre for Medium-Range Weather Forecasts (ECMWF), ERA Interim reanalysis data set. The wind forcing is updated at intervals of 6 simulated hours. A time series of the wind speed and direction at Sleipner A compared with data from Eklima project *www.met.no* is shown in Figure 2.

The tidal forcing applied on the open boundaries is taken from harmonic analysis and includes four tidal constituents; $M2$, $S2$, $K1$, and $N2$. Nodal factors and equilibrium arguments needed to get the phase and amplitude right for a given date comes from the ADCIRC model (*http://www.adcirc.org/*).

Fresh water runoff from 32 rivers around the North Sea and Norwegian coast originates from the Institute of Marine Research (IMR) and is the monthly mean discharge of the most significant rivers averaged over several years.

A full validation of the model set-up against in situ data has not been performed. The purpose here is not to do predictions of currents, or CO_2 concentrations, at a specific time or location, but to obtain heterogeneous statistics and probability fields. The model captures the well-known circulation patterns in the North Sea. Figure 3 shows transport of a passive tracer released in the central North Sea. The tracer concentration follows the expected circulation patterns with inflow of warm and saline Atlantic water from north continuing eastward. These saline and warm water masses mix with fresh water deep at Skagerak and then outflow with the Norwegian coastal current [*Rodhe*, 1998; *Otto* et al., 1990; *Winther and Johannessen*, 2006].

The time series of the current speed near bottom and surface at Sleipner A are presented in Figure 4. The current is dominated by the semi diurnal tidal signal with an average speed close to 10 cm/s, and an amplitude less than 10 cm/s. This corresponds well to published measurements in *Tryggestad et al.* [1983] reporting an average current speed around 10 cm/s with amplitudes between 10 and 20 cm/s.

Figure 5 presents a comparison between the observed and modeled mean salinity and temperature at Ytre Utsira measurement station and the nearest grid point. The observed salinity and temperature data are collected from the Institute of Marine Research website *http://www.imr.no*. As the forcing does not include surface heat flux, the modeled temperature near the surface has a zero gradient.
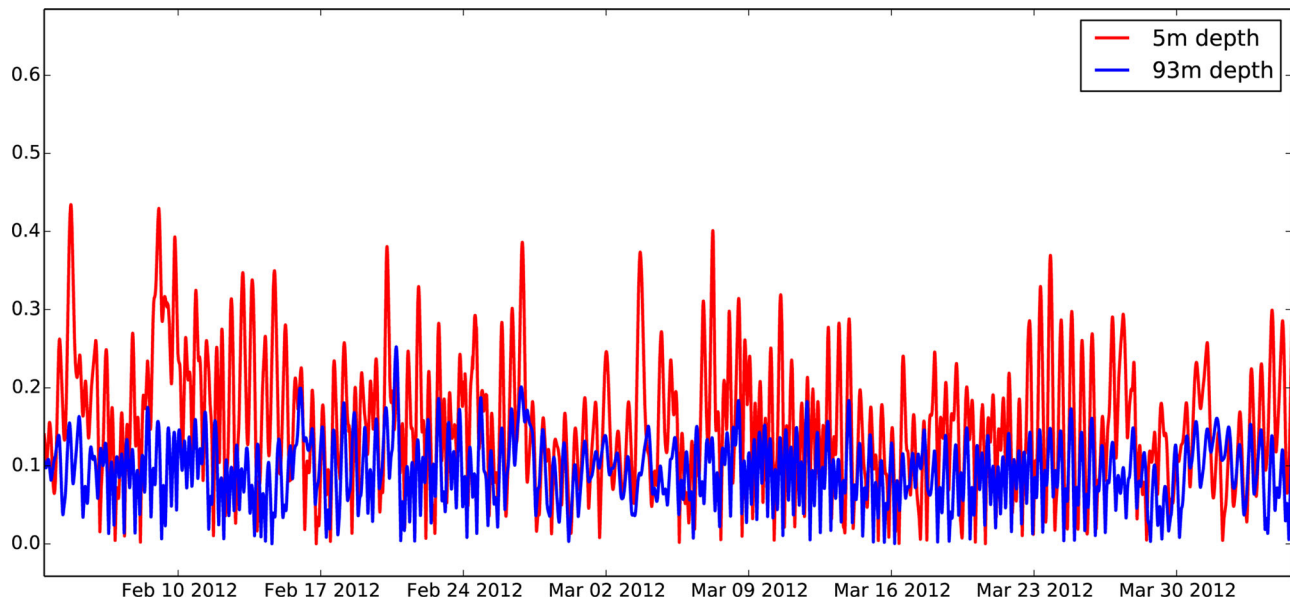
Figure 4. Current speed (m/s) at Sleipner A at depths of 5 m (red line) and 93 m (blue line).

3. Seep Simulations

Having confidence that the model includes current variability believed to be representative for the area, the model setup is used to predict how a CO_2 signal varies in time and space. The month of January is used to spin up the model, and the CO_2 sources are introduced at the first day of February until the end of March.

Under the assumption that the CO_2 signal is diluted enough to not have influence on the seawater density, the concentration can be simulated as a passive tracer. Therefore, the transport of CO_2 concentration, C, is modeled by an in-line advection-diffusion equation:

$$\frac{\partial C}{\partial t} + \vec{U} \cdot \nabla C = \frac{\partial}{\partial z}\left(K_H \frac{\partial C}{\partial z}\right) + \frac{\partial}{\partial x}\left(A_H \frac{\partial C}{\partial x}\right) + \frac{\partial}{\partial y}\left(A_H \frac{\partial C}{\partial y}\right) + Q \tag{1}$$

where Q represents leakage source. $\vec{U} = (U, V, W)$ is the velocity field, where U, V and W represent the velocities in x, y, and z directions. The horizontal diffusivity A_H is computed following *Smagorinsky* [1963], while
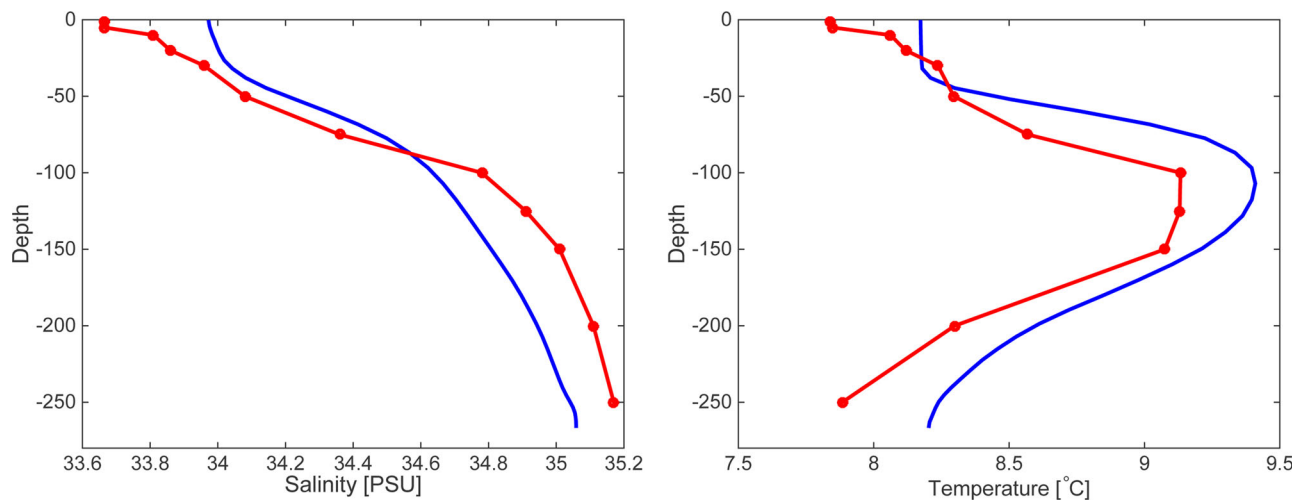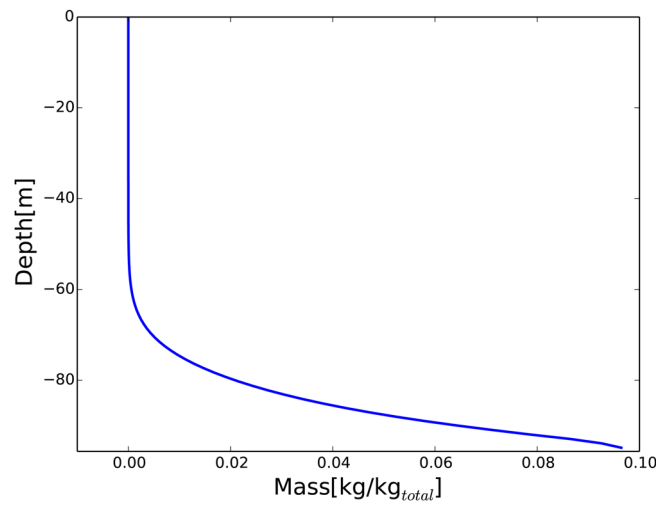

Figure 5. Vertical profiles of (left) salinity and (right) temperature representing January mean at Ytre Utsira station. Red line indicates the observed data and the blue line indicates BOM output.

Figure 6. Vertical profile of the normalized mass distribution (kg/kg total), for the Chimney reactivation scenario used as input to the BOM simulations. The profile is collected from *Alendal et al.* [2014] and represent results from the Heriot-Watt bubble plume model *Dewar et al.* [2013, 2015].

the vertical diffusivity coefficient is estimated using a turbulent closure described by *Mellor and Yamada* [1982].

As source term one of the scenarios from [*Alendal et al.*, 2014] with a CO_2 flux $Q \sim 150$ T/d, representing the chimney reactivation, has been used. The CO_2 is vertically distributed according to the results from the HWU model [*Dewar et al.*, 2013, 2015] as shown in Figure 6.

Nine independent seep locations are simulated, labeled C1, C2, C3,…,C9, in Figure 7, with C1 being at the center and located at Sleipner A with a global coordinate 1.94°E 58.36°N. The distance between each seep and its nearest neighbor is 10 grid cells, equivalent to 8 km. Each of these seeps uses the source profile given in Figure 6, implying that a leak in any of these locations will result in the same flux and vertical profile of dissolved CO_2. Each of the seeps is treated as a separate tracer, hence nine tracers are being advected through individual versions of equation (1). For each of these tracer fields time series are collected in a grid consisting of 53×51 neighboring grid cells, centered in the respective source point.

Figure 7 shows the average and standard deviation of the nine concentration fields at the seafloor. It is clear that there is a spatial dependency both in the average signal and the variability of the signal. The temporal variability is also high, as illustrated in Figure 8 showing snapshots of the C1 concentration field. This figure also reveals how topography influences in current conditions, and hence tracer transport.

The concentration time series for C1 in the grid cells adjacent to the seep location (centre) are shown in Figure 9, the red line marking the threshold concentration given by $C_t = 5 \, \mu mol/kg_{SW}$ [*Botnen et al.*, 2015]. A sensor located at the leak location will detect the seep when the concentration always is over the threshold. The differences between the time series in the upper and lower row are significant and the anisotropy is evident. Notice that the upper middle plot is not straight north of the seep. The model grid is rotated relative to latitude and longitude as can be seen in Figure 7.
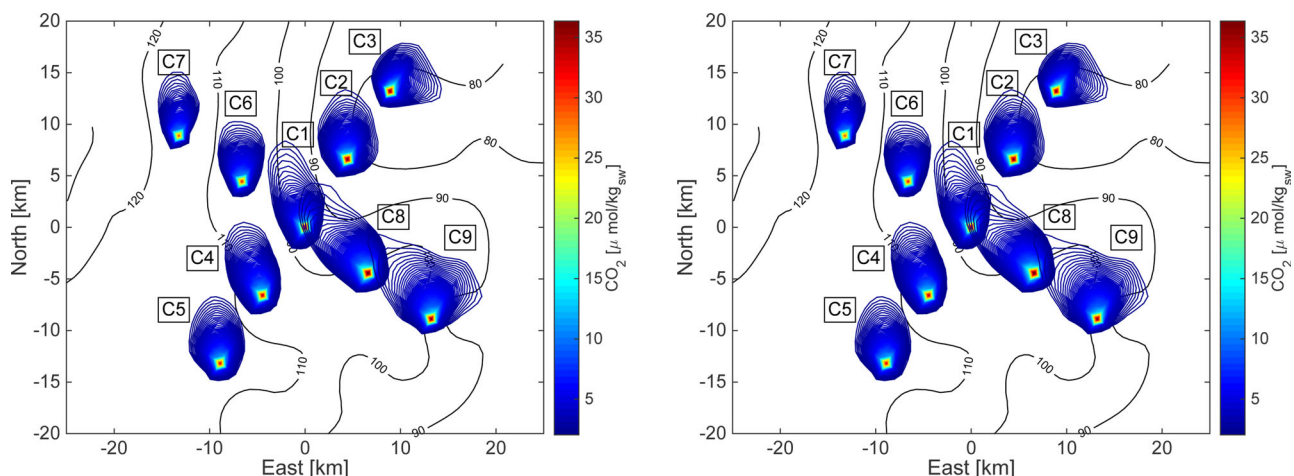
Figure 7. Contour plot of the (left) mean and (right) standard deviation of CO_2 concentration along the bottom for Chimney scenario released at nine locations labeled C1, C2, C3,…, C9.
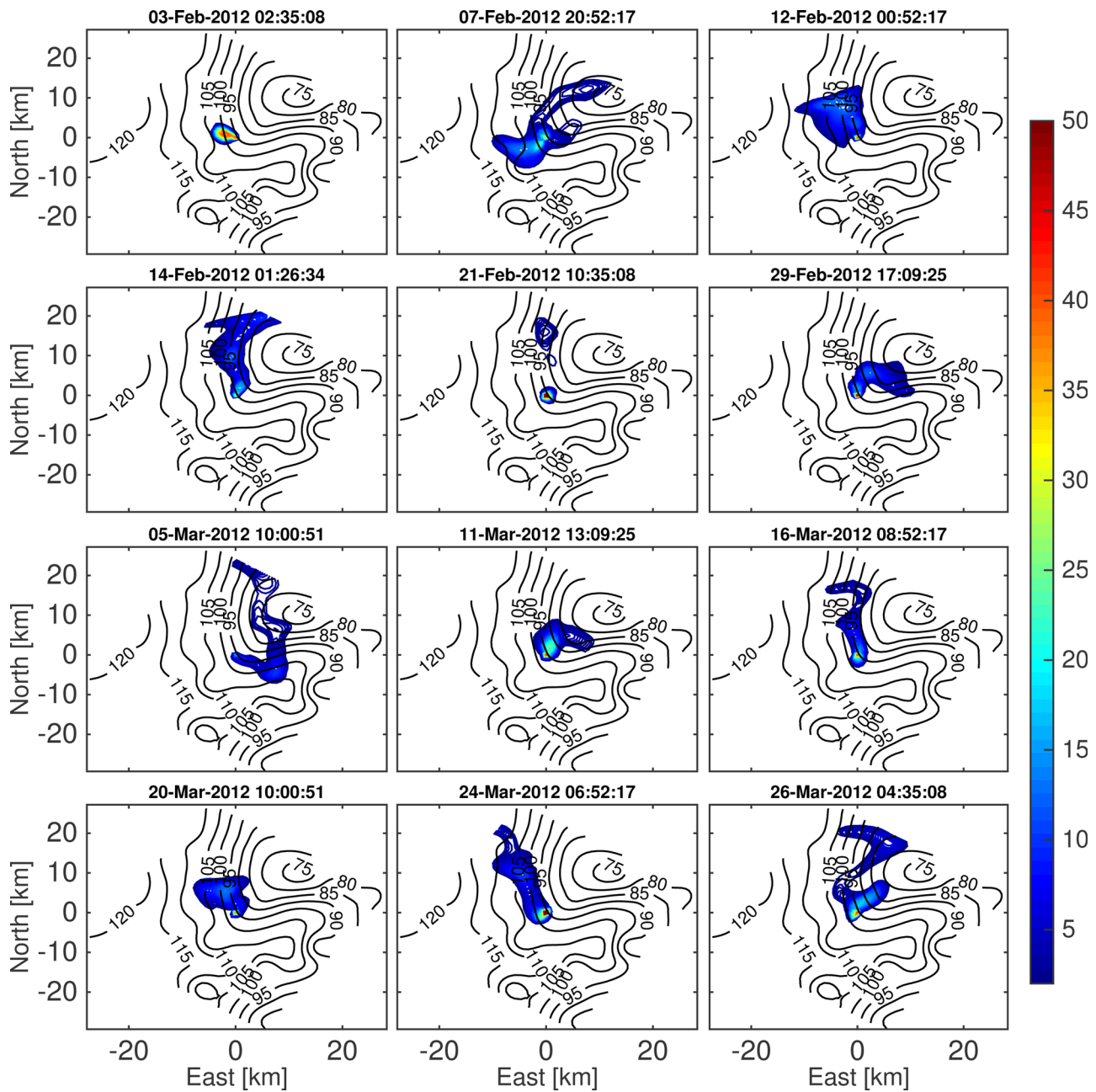
Figure 8. Temporal snapshots of the instant CO_2 concentration footprint along the seabed at different times for a seep at location C1. The CO_2 flux is continuous and starts at 12:00 on 1 February 2012. The unit for the colorbar is μmol/kgsw.

As a further illustration, the cumulative probability distributions of CO_2 concentration are shown in Figure 10. At the source (middle plot), the concentration stays above 10 μmol/kg$_{SW}$ almost 100% of the time, while it stays above 40 μmol/kg$_{SW}$ 20% of the time. Moving away from this source, these values decrease quickly in the neighboring grid cells (Figure 10), but it still reaches 10 μmol/kg$_{SW}$ 10% of the time in the first column and last row.

The heterogeneity of the signal is even more evident in Figure 11 showing contour lines as boundaries to the areas in which the concentration stays above the threshold value $C_t = 5$ μmol/kg$_{SW}$ [*Botnen et al.*, 2015] for a given percentage of the time. As can be seen, the size and shape of such areas for C1,C2...,C9 seeps are highly dependent on current and local topography. These fields represent the input needed in the monitor design framework presented in *Hvidevold et al.* [2015] and *Frøysa* [2015].
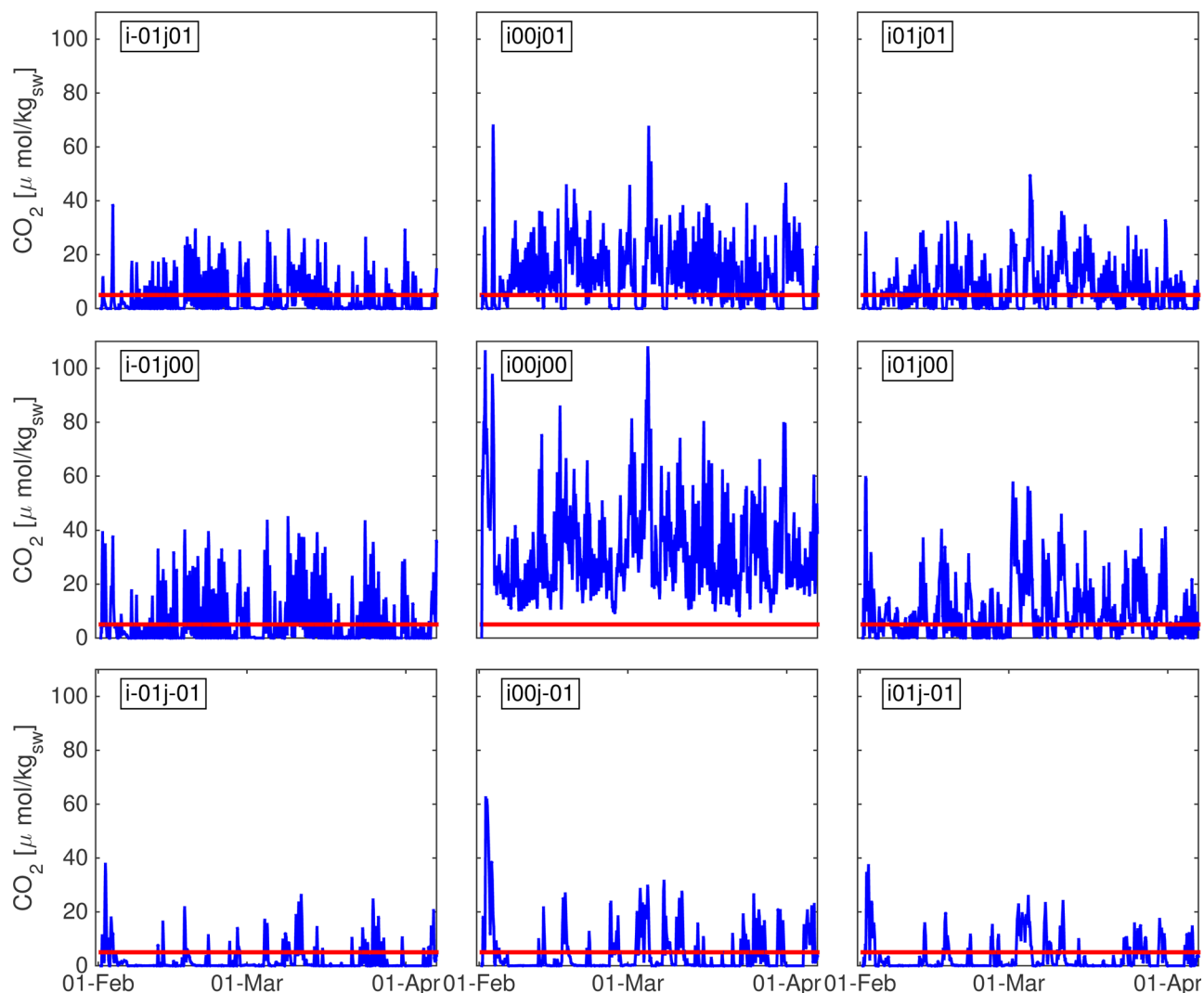
Figure 9. Time series of the CO_2 concentration along the seafloor at the (center panel) leak grid cell and the eight neighboring grid cells. The red line indicates the threshold value $C_t = 5$ μmol/kgsw [*Botnen et al.*, 2015].

4. Consequences for Designing a Monitoring Program

To illustrate how the heterogeneous footprint characteristics influence on monitoring design the framework described in *Hvidevold et al.* [2015] and *Frøysa* [2015] is used to design a monitoring program consisting of an array of chemical sensors at fixed locations.

It is assumed that there is an ongoing seep from an unknown location within the area shown in Figure 7. For simplicity, it is also assumed that the vicinity of each Ci has the same 10%, chance of being the seep location with a local probability leveling off toward a general background probability of 10% chance of the seep coming from another location. The resulting normalized probability map is shown in Figure 12 (top left plot).

A sensor is assumed to detect a seep if the seep results in a CO_2 concentration above $C_t = 5$ μmol/kg$_{SW}$ at the sensor location more than 10% of the time. This implies that the nine simulated seeps are assumed to be detectable in the area bounded by the blue contours in Figure 11. For other seep locations, a detectable region is obtained by interpolating the footprints using distance from the nine simulated.

Having a detectable region for all points in the grid, the next step is to find the region monitored by an arbitrarily placed sensor. This monitored region will be all seep locations for which the sensor is located inside
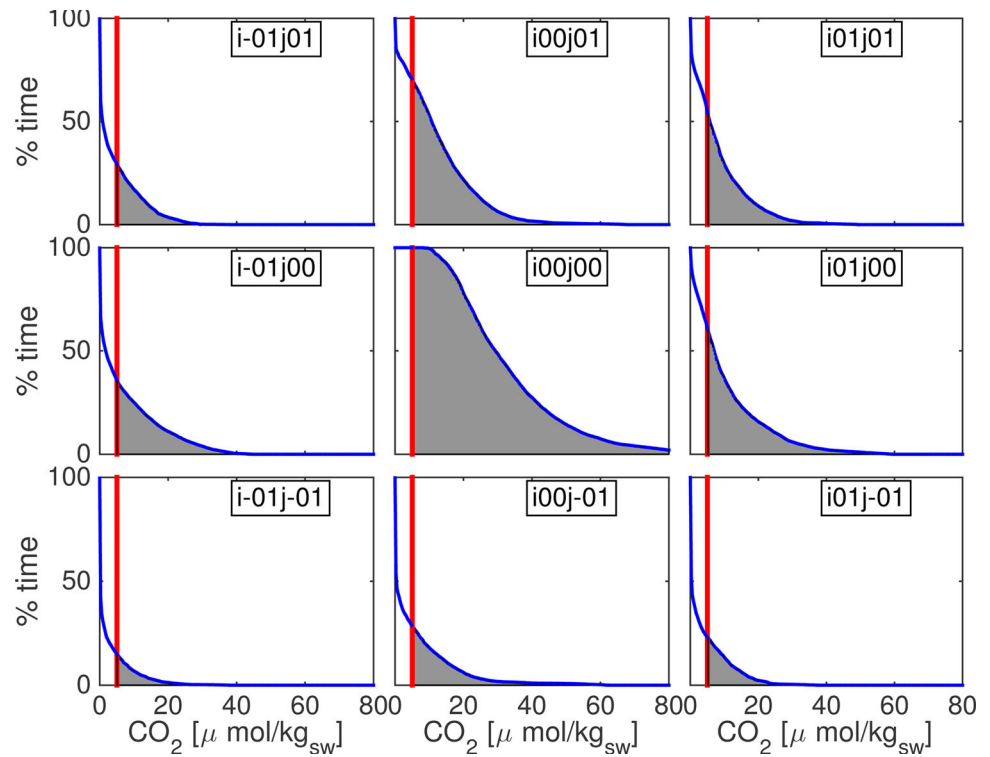
Figure 10. For all plots, the y axis represents the time percentage during which the CO_2 concentration stays above the value in the x axis, at the (center panel) leak grid cell and the eight neighboring grid cells. The red line indicates the threshold value $C_t = 5$ μmol/kgsw [*Botnen et al.*, 2015].
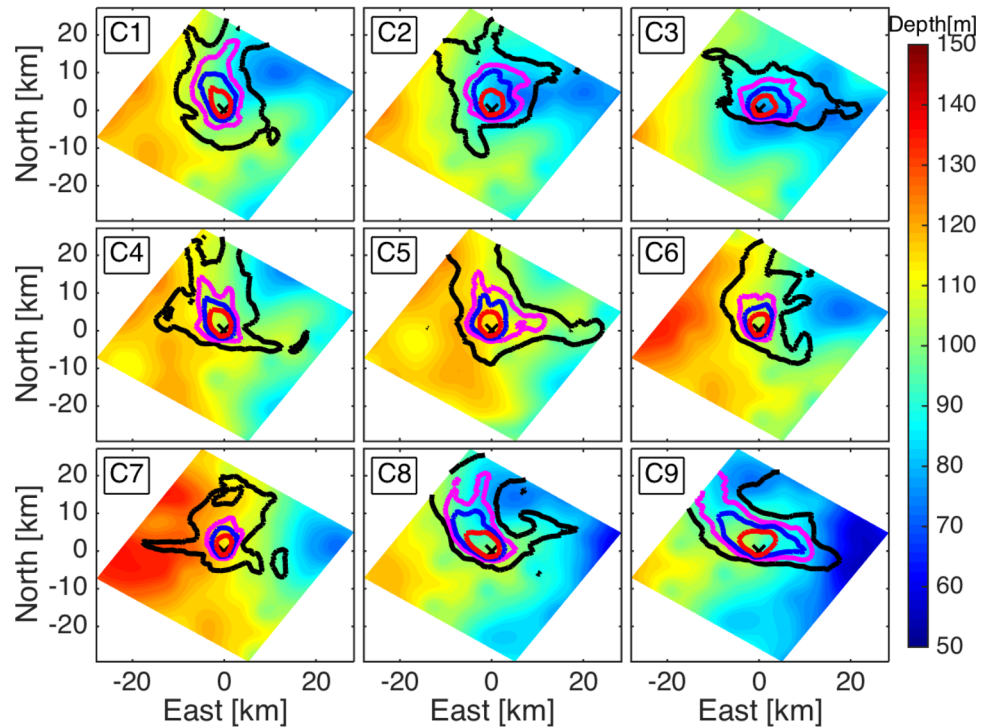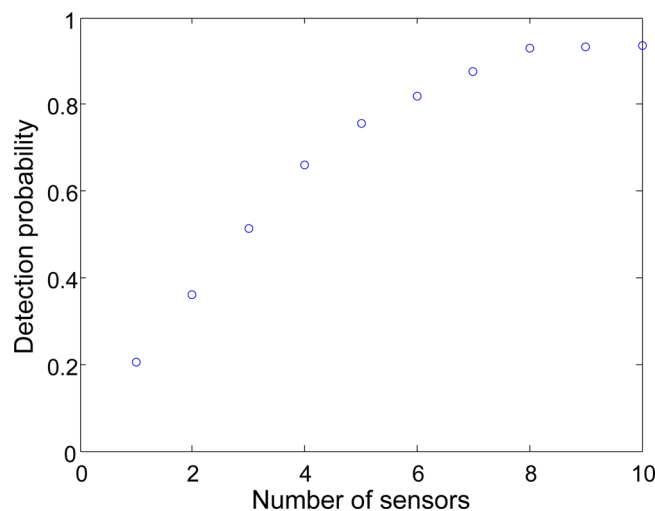

Figure 11. The contour lines indicate the area in which the CO_2 concentration stays above the threshold value $C_t = 5$ μmol/kgsw for 1% (black line), 5% (magenta line), 10% (blue line), and 20% (red line) of the total time. The background color represents the bathymetry in meters.
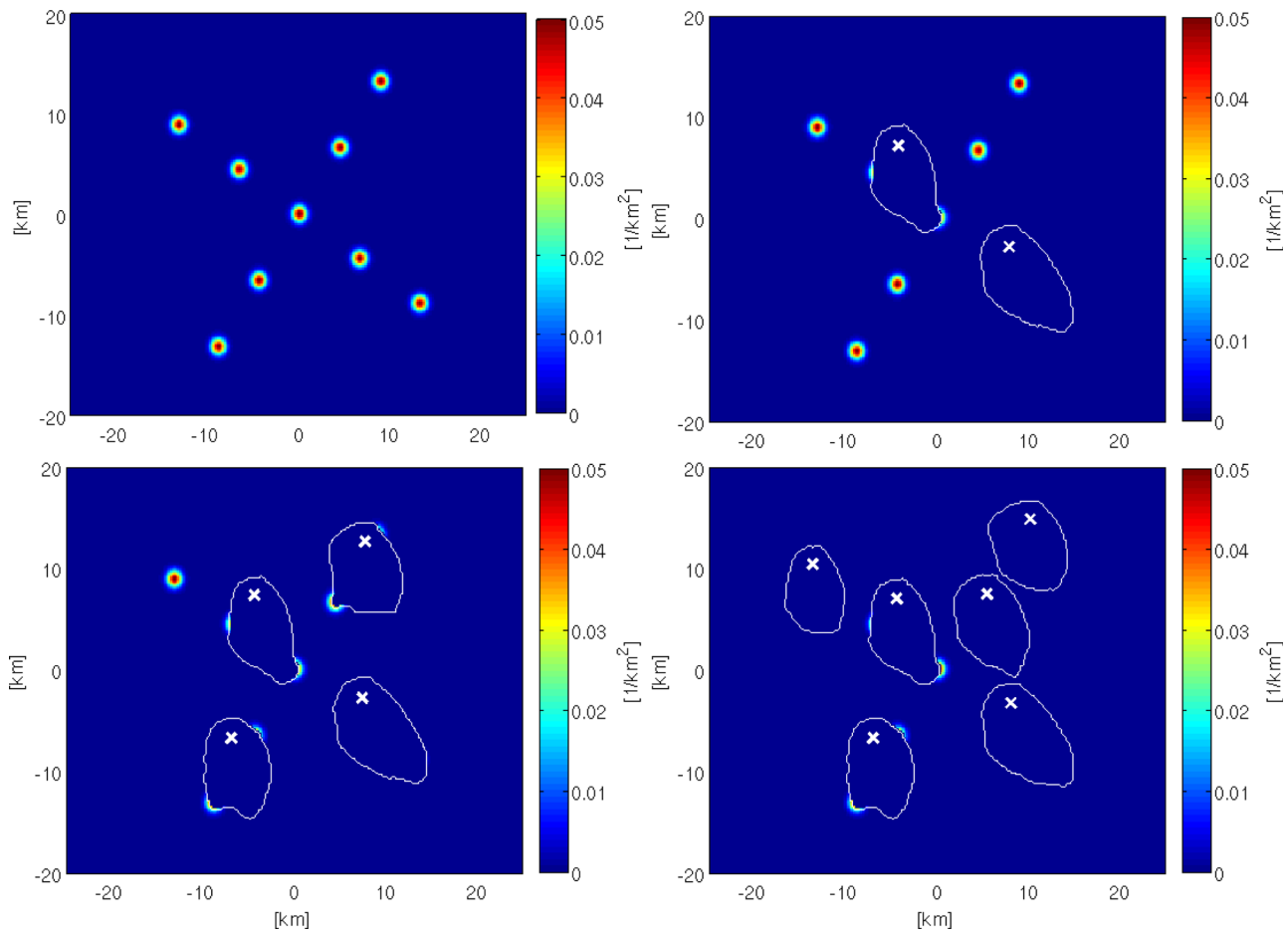
Figure 12. Designing a monitoring program. Each location (top left) has 10% probability of being the location of the leak, with a general background probability of 10%. The area monitored by the individual sensor located is indicated by the white outline for (top right) two, (bottom left) 4, and (bottom right) 6 sensors.

the detectable region, inverting the footprints in Figure 11 through a 180 degrees rotation. The probability of detecting the seep will hence be the sum of the seep locations within the monitored region weighted with the individual location's likelihood of being the seep location.

The optimal spatial layout of sensors, i.e., location of individual sensors, will be interdependent. If for instance two sensors have overlapping detection areas, the efficiency of the layout might not be optimal. This leads to the optimization problem of finding the optimal sensor layout maximizing the detection probability [*Hvidevold et al.*, 2015; *Frøysa*, 2015].

Results using Genetic Algorithm to find the optimal placements of two (top right), four (bottom left), and six (bottom right) sensors are shown in Figure 12. The white outlines represent boundaries of area monitored by

Figure 13. The resulting detection probability as function of number of sensors.

the respective sensors located at the white crosses. Notice how these change for the different sensor locations, especially evident in the bottom right plot.

Focusing on two sensors, Figure 12 (top right plot), each of them are placed to cover two high probability seep locations without being placed at the location of either of them. The lower right sensor covers two locations fully, while the upper is not able to rule out a leak in the vicinity of the two locations being monitored. The same is seen when increasing the number of sensors to four in Figure 12 (bottom left plot).

Also notice how the positioning of the uppermost sensor changes location and form of the monitored area as the number of sensor increases from four (bottom left) to six (bottom right) sensors.

Figure 13 shows the detection probability of the optimal sensor layout as function of the number of sensors. With all the assumptions and simplifications made, the numbers should be used with care. However, using a single footprint prediction independently of seep location will cause less accurate predictions and less confidence in the monitoring design.

5. Discussion

In this study, the same vertical profile of dissolved CO_2 has been used for the nine locations. In reality current conditions will have some influence on bubble plume behavior. Further, only one flux rate has been studied. When designing a real monitoring program, the different leak scenarios have to be incorporated, including the internal probability ratios between them. Also the flux rates will be different at an open well compared with a diffusive seep through sediments. Hence, also the source terms used will have spatial and temporal variability.

Only 2 months, using 2012 forcing, have been simulated. This is evidently not enough to build proper current and probable footprint statistics. In addition to longer and more thorough numerical simulations, the predictions will have to rely on in situ environmental statistics. Again stressing the need for a proper environmental baseline and site characterization.

With proper incorporation of spatial variability of leak characteristics, monitor programs allow for more reliable monitoring design, potentially also less costly. Higher confidence in the program, and quantification of degree of certainty when it indicates that a leak occurs, might reduce the amount of false alarms. An indication of a leak will trigger the next level of activity, locating the leak. This will include mobilizing extra resources, including costly surveys to the area. On the other hand, it is necessary to act on indications of leaks in order to identify and mitigate impacts.

References

Alendal, G., and H. Drange (2001), Two-phase, near-field modeling of purposefully released CO_2 in the ocean, *J. Geophys. Res.*, *106*(C1), 1085–1096.

Alendal, G., J. Berntsen, E. Engum, G. K. Furnes, G. Kleiven, and L. I. Eide (2005), Influence from ''Ocean Weather'' on near seabed currents and events at Ormen Lange, *Mar. Pet. Geol.*, *22*(1–2), 21–31.

Alendal, G., M. Dewar, A. Ali, Y. Evgeniy, L. Vielstädte, H. Avlesen, and B. Chen (2014), Technical report on environmental conditions and possible leak scenarios in the North Sea, *Tech. Rep. D3.4*, ECO2 deliverables , Univ. of Bergen, Bergen, Norway, doi:10.3289/ECO2_D3.4.

Berntsen, J. (2004), Users guide for a modesplit sigma-coordinate numerical ocean model, technical report, Dep. of Math., Univ. of Bergen, Bergen, Norway.

Berntsen, J., and E. Svendsen (1999), Using the SKAGEX dataset for evaluation of ocean model skills, *J. Mar. Syst.*, *18*(4), 313–331, doi.10.1016/S0924-7963(97)00,111-5.

Berntsen, J., J. Xing, and G. Alendal (2006), Assessment of non-hydrostatic ocean models using laboratory scale problems, *Cont. Shelf Res.*, *26*, 1433–1447.

Berntsen, J., J. Xing, and A. M. Davies (2008), Numerical studies of internal waves at a sill: Sensitivity to horizontal size and subgrid scale closure, *Cont. Shelf Res.*, *28*, 1376–1393.

Berntsen, J., J. Xing, and A. M. Davies (2009), Numerical studies of flow over a sill: Sensitivity of the non-hydrostatic effects to the grid size, *Ocean Dyn.*, *59*, 1043–1059.

Blackford, J. C., S. Widdicombe, D. Lowe, and B. Chen (2010), Environmental risks and performance assessment of Carbon Dioxide (CO_2) leakage in marine ecosystems, in *Developments and Innovation in Carbon Dioxide (CO_2) Capture and Storage Technology, Volume 2: Carbon Dioxide (CO_2) Storage and Utilisation*., pp. 344–373, Woodhead Publishing, CRC press, Cambridge, U. K.

Blackford, J., M. Haeckel, and K. Wallmann and ECO2 project (2012), Report on range of long-term scenarios to be simulated, *Tech. Rep. D12.2*., ECO2 deliverables, Plymouth Marine Laboratory, Plymouth, U. K., doi:10.3289/ECO2_D12.2.

Botnen, H. A., A. M. Omar, I. Thorseth, T. Johannessen, and G. Alendal (2015), The effect of submarine CO_2 vents on seawater: Implications for detection of subsea carbon sequestration leakage, *Limnol. Oceanogr.*, *60*(2), 402–410.

Boyd, A. D., Y. Liu, J. C. Stephens, E. J. Wilson, M. Pollak, T. R. Peterson, E. Einsiedel, and J. Meadowcroft (2013), Controversy in technology innovation: Contrasting media and expert risk perceptions of the alleged leakage at the Weyburn carbon dioxide storage demonstration project, *Int. J. Greenhouse Gas Control*, *14*, 259–269.

Brewer, P. G., B. Chen, R. Warzinki, A. Baggeroer, E. T. Peltzer, R. M. Dunk, and P. Walz (2006), Three-dimensional acoustic monitoring and modeling of a deep-sea CO_2 droplet cloud, *Geophys. Res. Lett.*, *33*, L23607, doi:10.1029/2006GL027181.

Caldeira, K., and M. E. Wickett (2003), Oceanography: Anthropogenic carbon and ocean pH, *Nature*, *425*(6956), 365–365.

Chen, B., Y. Song, M. Nishio, and M. Akai (2003), Large-eddy simulation of double cloud formation induced by CO_2 dissolution in the ocean, *Tellus, Ser. B*, *55*, 723–730.

Davies, A. M., and G. K. Furnes (1980), Observed and computed M_2 tidal currents in the North Sea, *J. Phys. Oceanogr.*, *10*(2), 237–257.

Dewar, M., W. Wei, D. McNeil, and B. Chen (2013), Small-scale modelling of the physiochemical impacts of CO_2 leaked from sub-seabed reservoirs or pipelines within the North Sea and surrounding waters, *Mar. Pollut. Bull.*, *73*(2), 504–515.

Dewar, M., N. Sellami, and B. Chen (2015), Dynamics of rising CO_2 bubble plumes in the QICS field experiment, *Int. J. Greenhouse Gas Control*, *38*, 52–3 doi:10.1016/j.ijggc.2014.11.003.

Frøysa, H. G. (2015), Design of a monitoring program in a varying marine environment, Master's thesis, Dep. of Math., Univ. of Bergen, Bergen, Norway. [Available at http://bora.uib.no.]

Greenwood, J., P. Craig, and N. Hardman-Mountford (2015), Coastal monitoring strategy for geochemical detection of fugitive CO_2 seeps from the seabed, *Int. J. Greenhouse Gas Control*, *39*, 74–78.

Hvidevold, H. K., G. Alendal, T. Johannessen, and A. Ali (2015), Survey strategies to quantify and optimize detecting probability of CO_2 seep in a varying marine environment, Manuscript resubmitted to Environ. Model. Softw.

Martinsen, E. A., and H. Engedahl (1987), Implementation and testing of a lateral boundary scheme as an open boundary condition for a barotropic model, *Coastal Eng.*, *11*, 603–637.

Mellor, G., and T. Yamada (1982), Development of a turbulence closure model for geophysical fluid problems, *Rev. Geophys. Space Phys.*, *20*, 851–875.

Noble, R. R. P., L. Stalker, S. A. Wakelin, B. Pejcic, M. I. Leybourne, A. L. Hortle, and K. Michael (2012), Biological monitoring for carbon capture and storage: A review and potential future developments, *Int. J. Greenhouse Gas Control*, *10*, 520–535.

Oldenburg, C. M., and J. L. Lewicki (2006), On leakage and seepage of CO_2 from geologic storage sites into surface water, *Environ. Geol.*, *50*(5), 691–705.

Otto, L., J. T. F. Zimmerman, G. K. Furnes, M. Mork, R. Sætre, and G. Becker (1990), Review of the physical oceanography of the North Sea, *Neth. J. Sea Res.*, *26*, 161–238.

Rodhe, J. (1998), The Baltic and North Seas: A process-oriented review of the physical oceanography, in *The Sea*, vol. 11, edited by A. R. Robinson, and K. H. Brink, pp. 699– 732, John Wiley, Hoboken, N. J.

Rutqvist, J. (2012), The geomechanics of CO_2 storage in deep sedimentary Formations, *Geotech. Geol. Eng.*, *30*(3), 525–551.

Rygg, K., G. Alendal, and P. M. Haugan (2011), Flow over a rounded backward-facing step, using a z-coordinate model and a sigma-coordinate model, *Ocean Dyn.*, *61*(10), 1681–1696.

Sato, T., and K. Sato (2002), Numerical prediction of the dilution process and its biological impacts in CO_2 ocean sequestration, *J. Mar. Sci. Technol.*, *6*(4), 169–180.

Smagorinsky, J. (1963), General circulation experiments with the primitive equations, i. The basic experiment, *Mon. Weather Rev.*, *91*, 99–164.

Thiem, Ø., M. Carr, J. Berntsen, and P. Davies (2011), A numerical simulation of internal solitary wave - induced reverse flow and associated vortices in a shallow, two-layer fluid benthic boundary layer, *Ocean Dyn.*, *61*(6), 857–872.

Tryggestad, S., K. A. Selanger, J. P. Mathisen, and Ø. Johansen (1983), Extreme bottom currents in the North Sea, in *North Sea Dynamics*, edited by J. Sundermann and W. Lenz pp. 148–158, Springer.

Wegener, G., M. Shovitri, K. Knittel, H. Niemann, M. Hovland, and A. Boetius (2008), Biogeochemical processes and microbial diversity of the Gullfaks and Tommeliten methane seeps (Northern North Sea), *Biogeosci. Discuss.*, *5*(1), 971–1015.

Winther, N. G., and J. A. Johannessen (2006), North Sea circulation: Atlantic inflow and its destination, *J. Geophys. Res.*, *111*, C12018, doi: 10.1029/2005JC003,310.